CONTRACT REPORT BRL-CR-595

BRL

1938 – Serving the Army for Fifty Years – 1988

A NEW COMPUTATIONAL CAPABILITY FOR RAMJET PROJECTILES

ROCKWELL INTERNATIONAL
SCIENCE CENTER
1049 CAMINO DOS RIOS
THOUSAND OAKS, CA 91360

MARCH 1988

U.S. ARMY LABORATORY COMMAND

BALLISTIC RESEARCH LABORATORY

ABERDEEN PROVING GROUND, MARYLAND

DESTRUCTION NOTICE

Destroy this report when it is no longer needed. DO NOT return it to the originator.

Additional copies of this report may be obtained from the National Technical Information Service, U.S. Department of Commerce, Springfield, VA 22161.

The findings of this report are not to be construed as an official Department of the Army position, unless so designated by other authorized documents.

The use of trade names or manufacturers' names in this report does not constitute indorsement of any commercial product.

UNCLASSIFIED
SECURITY CLASSIFICATION OF THIS PAGE

REPORT DOCUMENTATION PAGE

Form Approved
OMB No. 0704-0188

1a. REPORT SECURITY CLASSIFICATION UNCLASSIFIED	1b. RESTRICTIVE MARKINGS
2a. SECURITY CLASSIFICATION AUTHORITY	3. DISTRIBUTION/AVAILABILITY OF REPORT Approved for public release; distribution is unlimited.
2b. DECLASSIFICATION/DOWNGRADING SCHEDULE	
4. PERFORMING ORGANIZATION REPORT NUMBER(S) SC5462.FR	5. MONITORING ORGANIZATION REPORT NUMBER(S) BRL-CR-595
6a. NAME OF PERFORMING ORGANIZATION Rockwell International Science Center 6b. OFFICE SYMBOL (If applicable)	7a. NAME OF MONITORING ORGANIZATION
6c. ADDRESS (City, State, and ZIP Code) 1049 Camino Dos Rios Thousand Oaks, CA 91360	7b. ADDRESS (City, State, and ZIP Code)
8a. NAME OF FUNDING/SPONSORING ORGANIZATION U.S. Army Ballistic Research Laboratory 8b. OFFICE SYMBOL (If applicable) SLCBR-LF	9. PROCUREMENT INSTRUMENT IDENTIFICATION NUMBER Contract No. DAAA15-86-C-0053
8c. ADDRESS (City, State, and ZIP Code) Aberdeen Proving Ground, MD 21005-5066	10. SOURCE OF FUNDING NUMBERS PROGRAM ELEMENT NO. / PROJECT NO. / TASK NO. / WORK UNIT ACCESSION NO.

11. TITLE (Include Security Classification)
A NEW COMPUTATIONAL CAPABILITY FOR RAMJET PROJECTILES

12. PERSONAL AUTHOR(S)
Chakravarthy, S.R.

13a. TYPE OF REPORT	13b. TIME COVERED	14. DATE OF REPORT (Year, Month, Day)	15. PAGE COUNT
Final Report	FROM 05/86 TO 04/87	1987 September	28

16. SUPPLEMENTARY NOTATION "The view, opinions, and/or findings contained in this report are those of the author and should not be construed as an official Department of the Army position, policy or decision, unless so designated by other documentation."

17. COSATI CODES			18. SUBJECT TERMS (Continue on reverse if necessary and identify by block number)
FIELD	GROUP	SUB-GROUP	
21	05		
19	01		

19. ABSTRACT (Continue on reverse if necessary and identify by block number)

A state-of-the-art computer code has been applied to calculate internal and external flows for a ramjet projectile under turbulent, supersonic conditions. A multizone computational approach has been used, and its advantages are demonstrated. Two turbulence modeling approaches were tried: (1) the Baldwin-Lomax model applied throughout the flow field; (2) the Baldwin-Lomax model applied outside of backflow regions and a dedicated algebraic k-ε backflow model applied within these regions. Comparison with experimental data shows a significant improvement in the code's predictional capability when the latter approach is used.

20. DISTRIBUTION/AVAILABILITY OF ABSTRACT ☐ UNCLASSIFIED/UNLIMITED ☒ SAME AS RPT. ☐ DTIC USERS	21. ABSTRACT SECURITY CLASSIFICATION UNCLASSIFIED
22a. NAME OF RESPONSIBLE INDIVIDUAL Dr. William P. D'Amico, Jr.	22b. TELEPHONE (Include Area Code) (301)-278-3405 22c. OFFICE SYMBOL SLCBR-LF-A

DD Form 1473, JUN 86 Previous editions are obsolete.

SECURITY CLASSIFICATION OF THIS PAGE
UNCLASSIFIED

Table of Contents

List of Figures

A NEW COMPUTATIONAL CAPABILITY FOR RAMJET PROJECTILES

Sukumar R. Chakravarthy and Uriel C. Goldberg

Rockwell International Science Center
Thousand Oaks, California

Abstract

A state–of–the–art computer code has been applied to calculate internal and external flows for a ramjet projectile under turbulent, supersonic conditions. A multizone computational approach has been used, and its advantages are demonstrated. Two turbulence modeling approaches were tried: 1) The Baldwin–Lomax model applied throughout the flow field; 2) The Baldwin–Lomax model applied outside of backflow regions and a dedicated algebraic k–ϵ backflow model applied within these regions. Comparison with experimental data shows a significant improvement in the code's predictional capability when the latter approach is used.

1. INTRODUCTION

Solid fuel ramjet technology is currently of high interest. Initial tests for spin–stabilized projectiles demonstrated the feasibility of the technology. However, many fundamental issues must still be resolved in order to properly exploit this emerging technology. For example, combustion efficiency as observed in flight is much lower than preliminarily predicted. This may be due to the spin of the projectile. On the other hand, the preliminary predictions may have been inaccurate because the internal flow and combustion processes of hollow ramjet projectiles are not completely understood. Without a thorough knowledge of such processes, scaling laws cannot be established to design new projectiles that may be fin or spin–stabilized. A series of "cold flow" wind tunnel tests (no combustion) have been conducted, and earlier numerical computations have not shown consistent agreement with the wind tunnel measurements. Wind tunnel tests are very expensive and new ramjet models can not be established solely on the basis of empirical data bases from previous flight histories and wind tunnel tests. New accurate and reliable numerical methods must be established to support the ramjet program.

Many numerical methods have artificial viscosity (sometimes called numerical smoothing or dissipation) controlled by selecting various coefficients. The presence of these terms

and their wide range of possible parameters are highly undesirable. Often individual solutions must be carefully fine tuned to achieve acceptable/stable solutions. These dissipative terms become very troublesome in high speed flow problems when turbulence models (which also have several adjustable constants) must be applied. The inherent complex geometries associated with solid fuel ramjets, together with these other problems, present a very difficult simulation problem. The number of free parameters within the numerical solution must be reduced to a minimum.

It is clear that numerical methods with more exact modeling (fewer adjustable or empirical terms) must be developed for the ramjet problem. Recently a new class of numerical methods has been developed that are more exact and reliable. These approaches have been termed total variation diminishing (TVD) formulations. Such numerical methods are under investigation by a few researchers for cases of inviscid flow and two–dimensional or simple geometries (ramjet problems need three dimensions, have nozzles, inlets, and other irregular geometrical features such as flame holders). The present authors have published these types of solutions, and have since produced a series of codes where viscous/turbulent/separated flow processes within complex geometries are treated. As will be shown in this paper, the presence or absence of an adequate turbulence model dedicated to the treatment of separated flow regions makes all the difference between satisfactory and poor predictional capability of the state–of–the–art computer code used in the present work.

2. COMPUTATIONAL APPROACH

The computational fluid dynamics (CFD) approach is to use state–of–the–art numerical algorithms based on the TVD formulation along with an implicit, factored time–stepping algorithm in a zonal grid framework. The TVD formulation contributes to a very reliable (no numerical oscillations, no "numerical" user knobs such as dissipation coefficients) and accurate methodology. The solution procedure using implicit schemes also contributes to computational efficiency. The use of zonal grids simplifies the construction of computational grids, allows complex topologies to be treated routinely and permits more options in working with limited computer main core memory, etc.

The TVD formulation is used to discretize the hyperbolic part of the Navier–Stokes equations. The diffusion components of these equations are treated with central difference approximations for second derivative terms in each direction. The cross–derivative terms are discretized in a novel fashion to augment the diagonal dominance of the resulting set of difference equations.

2.1 Computational Grid — A Zonal Approach

The problem of computing internal/external ramjet projectile flow fields is complicated by the complex geometry and the complex physics involved. Resolving the physics in complex geometries could necessitate the use of dense grids for which the required data storage might easily outstrip available in–core computer memory. In the present approach, a zonal grid is used to treat the ramjet internal/external flow geometries. This allows considerable flexibility in responding to the complexities of geometry, physics, and computer resources.

In the zonal approach, the computational method and the computer program are constructed in such a manner that each zone may be considered as a more–or–less independent module with the zones interacting with each other after or before the information corresponding to each zone is updated one cycle.

Complex geometries are gridded more easily by zonal approaches. The complete physical domain to be considered can be broken up into simpler topological subdivisions. Even a single topological subunit can be divided into many zones. Selective and adaptive grid refinement can be employed in some of these zones to increase accuracy and resolution.

Zonal approaches are also one way of reducing the required in–core computer memory. In such approaches, it would be sufficient to have enough main core storage to fit the needs of a single zone.

The usefulness of a particular grid can be verified by repeating the calculations on twice finer or coarser a grid and estimating the truncation error from the two sets of data. The zonal approach permits such an estimation to take place in a restricted region of the entire domain with an attendant saving in computational resources (both time and memory). Zonal approaches also permit the easy implementation of local refinement techniques. Specific regions of the flow field may be selected for additional refinement and can be treated as a new zone.

The multigrid strategy will be employed at a later stage to enhance computational efficiency even further. The multigrid method involves the use of a hierarchy of crude and fine grids in a cyclical pattern, the aim being to reduce the residue on the finest grid by performing calculations on coarser grids. The computer program organization required for multigrid techniques is identical to that required for zonal approaches and, thereby, the zonal approach enables a natural transition from zonal methods to zonal multigrid methods.

In each zone, any approach to generating the computational grid may be used: algebraic methods, differential equations methods, etc. In the latter category, elliptic or hyperbolic methods may be used, as applicable. The multisurface technique is representative of the former type of grid generation method.

This subsection on grid generation is now concluded by actually illustrating the multizone grid treatment for a ramjet projectile geometry. Figure 1 shows the division of the complete geometry into 6 zones. Figure 2 shows the composite 6–zone grid used for the calculations and consisting of the following meshes in Zones 1 through 6: 30×35, 7×17, 50×30, 30×17, 15×25, and 45×20. The grids have been generated in such a manner that the horizontal families of mesh lines within the projectile are continuous between zones and the vertical families are continuous in the zones external to the ramjet projectile. This type of grid is natural for the problem at hand but the computational methodology permits a wider class of patched zonal grids: neither family of grid lines need be continuous across zones.

2.2 Computational Algorithm

The computational discretization technique must be reliable and robust if it is to successfully capture the complex physics of ramjet internal and external flow fields. The TVD formulation for convection terms (the hyperbolic part of the time–dependent Navier–Stokes equations), along with a careful treatment of diffusion terms, offers itself as the best alternative.

TVD formulations are relatively new but well proven and documented[1–4]. By design, they have some desirable features: they are highly accurate (up to third–order accuracy for steady–state solutions to hyperbolic equations); they avoid numerical oscillations which could arise in high gradient regions, near shock waves, etc.; they avoid the formation of unphysical expansion shock waves; they contribute to the diagonal dominance of the finite difference equations. They are completely defined; there are no "numerical" dissipation and other coefficients to be tuned case by case. They have successfully been applied to compute a very wide range of inviscid and viscous flows without recourse to such "tuning knobs".

Proper treatment of diffusion terms that arise in the Navier–Stokes equations, in the equations of turbulence modeling, species equations of combustion chemistry, etc., are also important in the construction of reliable numerical methods. Unidirectional second derivative terms are conveniently handled correctly by using central difference approximations.

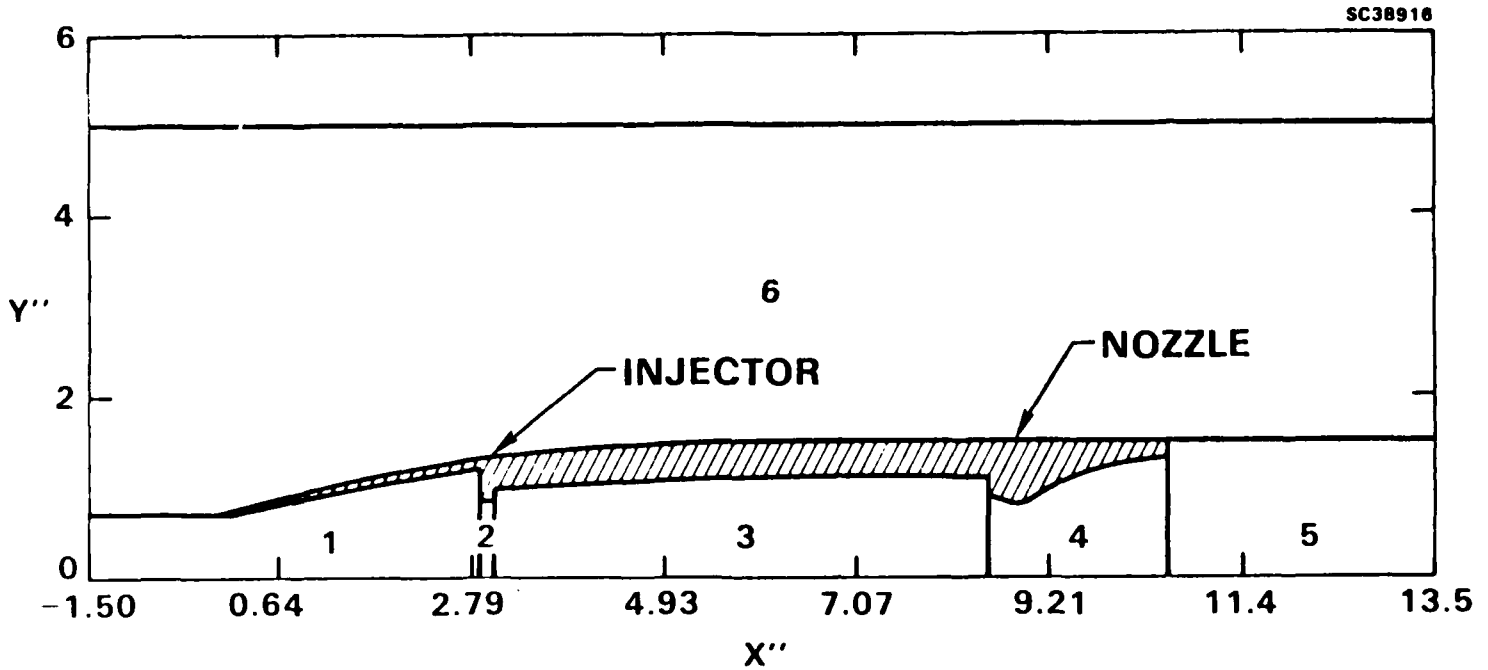

Fig. 1. 6-zone approach for ramjet projectile geometry

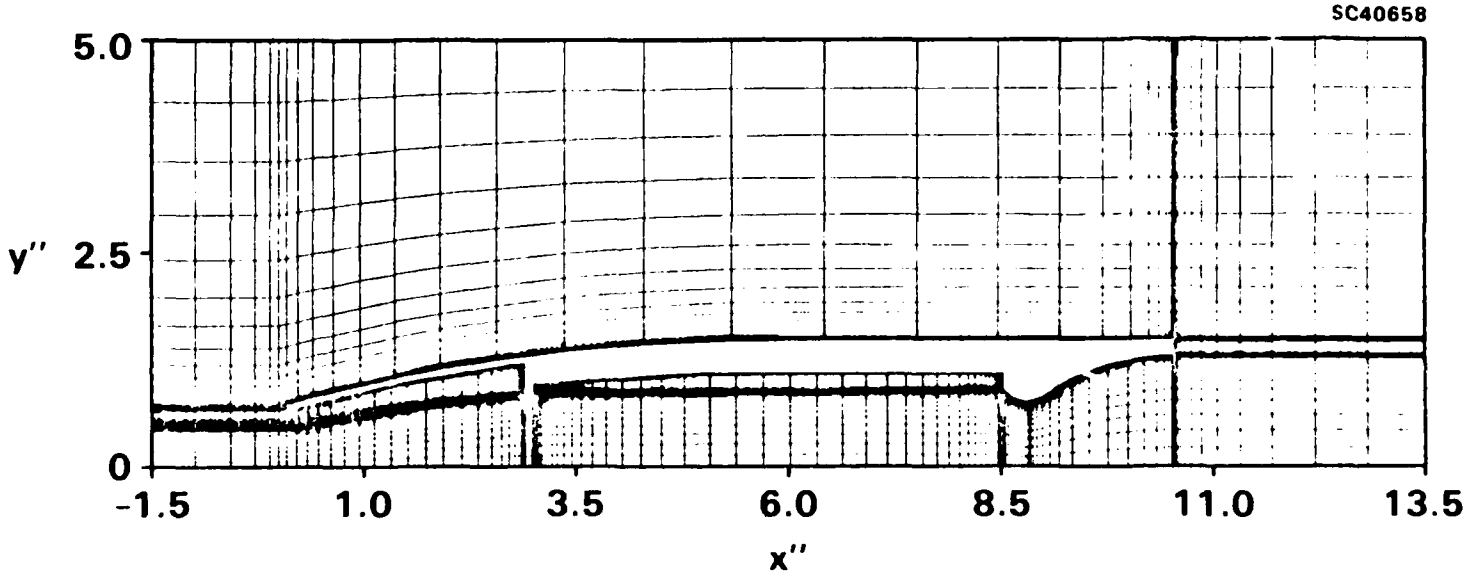

Fig. 2. 6–zone composite grid for ramjet projectile geometry

Cross derivatives are conventionally treated in cavalier fashion. In the present work, a careful cross derivative treatment which augments diagonal dominance is used[2]. Once again, this is a novel but proven technique which will contribute much to the reliability and robustness of the numerical procedure.

Conventional approximate factorization methods are used to handle multidimensional implicit formulations and this is the preferred approach in the present development. However, the diagonal dominance of TVD schemes (with properly discretized cross derivative terms) makes it possible to use relaxation methods[5].

Many techniques can be applied to implement an efficient code based on the above methods. The equations of turbulence modeling will be decoupled from the Reynolds-averaged Navier–Stokes equations in the implicit inversion procedure. This decoupling will have the effect of reducing the magnitude of the computational linear algebra problem of inverting a block tridiagonal system of equations and will not have a significant effect on the time accuracy of the overall numerical procedure. The entire code is "vectorized" (which involves a restructuring of FORTRAN loops, eliminating recursive and conditional statements in those loops, etc.) to a very high degree and will be, therefore, very suitable for high speed vector computers such as the CRAY–XMP. Other techniques which may be used selectively include: the use of spatially varying time steps to accelerate the solution to time–asymptotic steady states when possible; the use of "diagonalization" approaches in which the left–hand side of the implicit approximately factored form of the difference equations is preconditioned and the resulting equations are solved as a set of scalar equations. (This approach requires the viscous terms to be placed only on the right–hand side of the equations. It also has a side effect on the conservation property but only in the transient stages and not when steady state is reached.)

2.3 Equations of Motion

The compressible, Reynolds–averaged Navier–Stokes equations for 2D/axisymmetric flow are written in the following conservation form, where the dependent variables u, v, and e are mass–averaged, with e being the specific total internal energy, T the temperature, ρ and p being mean density and pressure, respectively, and t being time:

$$\frac{\partial W}{\partial t} + \frac{\partial F}{\partial x} + \frac{\partial G}{\partial y} + \left(\frac{G}{y} - \frac{H}{y}\right)\alpha = 0 \qquad (1a)$$

and

$$W = \begin{bmatrix} \rho \\ \rho u \\ \rho v \\ \rho e \end{bmatrix} \quad , \quad F = \begin{bmatrix} \rho u \\ \rho u^2 - \sigma_{xx} \\ \rho uv - \tau_{xr} \\ \rho ue + \dot{q}_x - \sigma_{xx}u - \tau_{xr}v \end{bmatrix}$$

$$G = \begin{bmatrix} \rho v \\ \rho uv - \tau_{xr} \\ \rho v^2 - \sigma_{rr} \\ \rho ve + \dot{q}_r - \tau_{xr}u - \sigma_{rr}v \end{bmatrix} \quad , \quad H = \begin{bmatrix} 0 \\ 0 \\ -\sigma_+ \\ 0 \end{bmatrix} \tag{1b}$$

where:

$$\sigma_{xx} = -p - \frac{2}{3}(\mu + \mu_t)\nabla \cdot U + 2(\mu + \mu_t)\frac{\partial u}{\partial x}$$

$$\sigma_{rr} = -p - \frac{2}{3}(\mu + \mu_t)\nabla \cdot U + 2(\mu + \mu_t)\frac{\partial v}{\partial y}$$

$$\sigma_+ = -p - \frac{2}{3}(\mu + \mu_t)\nabla \cdot U + 2(\mu + \mu_t)\frac{v}{y}\alpha$$

$$\tau_{rx} = \tau_{xr} = (\mu + \mu_t)\left(\frac{\partial u}{\partial y} + \frac{\partial v}{\partial x}\right)$$

$$e = C_v T + \frac{1}{2}(u^2 + v^2)$$

$$\dot{q}_x = -C_p\left(\frac{\mu}{\mathrm{Pr}} + \frac{\mu_t}{\mathrm{Pr}_t}\right)\frac{\partial T}{\partial x}$$

$$\dot{q}_r = -C_p\left(\frac{\mu}{\mathrm{Pr}} + \frac{\mu_t}{\mathrm{Pr}_t}\right)\frac{\partial T}{\partial y}$$

$$\nabla \cdot U = \frac{\partial u}{\partial x} + \frac{\partial v}{\partial y} + \frac{v}{y}\alpha \tag{1c}$$

$$\alpha = \begin{cases} 1, & \text{axisymmetric flow} \\ 0, & \text{two dimensional flow} \end{cases} \tag{1d}$$

In Eq. (1), the laminar and eddy viscosities, μ and μ_t, are implicitly divided by the reference Reynolds number. The equations used for the Euler calculations are obtained from Eq. (1) by setting both laminar and eddy viscosities to zero.

In all the calculations, the air was assumed to be a perfect gas, satisfying the equation of state

$$p = \rho RT. \tag{2}$$

The following power law was used to relate molecular viscosity to temperature[6]:

$$\mu/\mu_0 = (T/T_0)^n \tag{3}$$

where $\mu_0 = 0.1716$ mP, $T_0 = 491.6°\mathrm{R}$, and $n = 0.64874$.

The *laminar and turbulent Prandtl numbers*, Pr and Pr_t, were assumed constant with values of 0.72 and 0.9, respectively. The ratio of specific heats, γ, was also assumed constant and equal to 1.4. C_v and C_p are specific heat capacities at constant volume and constant pressure, respectively.

For time–invariant grids, in the ξ–η computational plane, Eq. (1a) is transformed into the finite volume conservation law form represented by[2]

$$\frac{\partial W}{\partial \tau} + \frac{1}{\text{Area}}\Big[(y_\eta F - x_\eta G)_\xi + (-y_\xi F + x_\xi G)_\eta + \frac{G}{y} - \frac{H}{y}\Big] = 0 \tag{4}$$

where ξ and η are the new independent variables and x_ξ, x_η, y_ξ, and y_η are the four transformation coefficients obtained numerically from the mapping procedure. The "Area" in Eq. (4) denotes the area of the finite volume cell under consideration at the time of discretization of the equations. τ denotes transformed time.

3. TURBULENCE MODELING

Ramjet internal flows involve large regions of recirculatory flow, induced both by shock waves and by sharp geometrical discontinuities. Most existing turbulence models either do not treat such regions or do so in an *ad hoc* fashion which is frequently inadequate. A notably different approach is the use of a full Reynolds stress closure model, involving the solution of five coupled partial differential equations (for two–dimensional flows) for the three normal stresses, the shear stress, and the length scale. These must be supplemented by a wall function to provide turbulence quantities across viscous regions adjacent to solid surfaces. Such a wall function is usually some form of the law–of–the–wall, which, according to experimental observations, does not apply to separated flows. Thus, an expensive and time consuming computation of the Reynolds stresses is coupled with a questionable near–wall formulation.

In an attempt to improve predictional capability of separated flows using current Reynolds–averaged Navier–Stokes codes, a new and simple turbulence model has recently been introduced[7], some details of which are given below.

3.1 Highlights of the Turbulence Model

The new turbulence model is based on experimental observations of separated turbulent flows. The model prescribes turbulence kinetic energy (k) and its dissipation (ϵ)

analytically inside separation bubbles. A Gaussian variation of k normal to walls is assumed. The length scale of turbulence within bubbles is proportional to the local distance from the wall to the edge of the viscous sublayer, which is located outside the backflow region, as shown in Fig. 3. The latter feature is a basic assumption of the model.

The velocity scale is the local maximum Reynolds stress, which typically occurs around the middle of the boundary layer, well outside the bubble. This scale must be supplied by a turbulence model which is used beyond separated regions.

The main equations of the backflow model are given in the Appendix. A simple formula for eddy viscosity distribution within separation bubbles results, and is used to supply eddy viscosity for the Reynolds-averaged equations when performing the calculations inside the bubbles. Outside, another turbulence model (*e.g.*, Baldwin–Lomax or k–ϵ) supplies the values of eddy viscosity. In all the calculations presented here, the Baldwin–Lomax model was applied outside backflow regions. In order to mimic the influence of the large eddies residing outside separation zones, the following averaging procedure is performed when switching from the separation model to the one used beyond backflows: outside backflows, normal to walls, the eddy viscosity is taken to be the average of the one supplied by the model used beyond backflows and that given by the separation model with $f = A + B$ (see Appendix); downstream of reattachment, the history effect of the large eddies is taken into account by averaging the locally predicted eddy viscosity with the one provided by the separation model at the location within backflows where the skin friction attains its maximum negative value.

The mutual influence of multiple walls on the eddy viscosity is taken into account by using an inverse averaging procedure:

$$\mu_t = \frac{\sum_{i=1}^{N} (\mu_t/n)_i}{\left(\sum_{i=1}^{N} 1/n_i^2\right)^{1/2}}$$

where N is the number of walls, n_i is the local normal distance from the i^{th} wall, and μ_{t_i} is the eddy viscosity due to the presence of the i^{th} wall by itself.

Further details about the new model and its performance are given in Refs. 7–9. It should be noted that the model is not of an eddy viscosity type; it can be used in conjunction with Reynolds stress models.

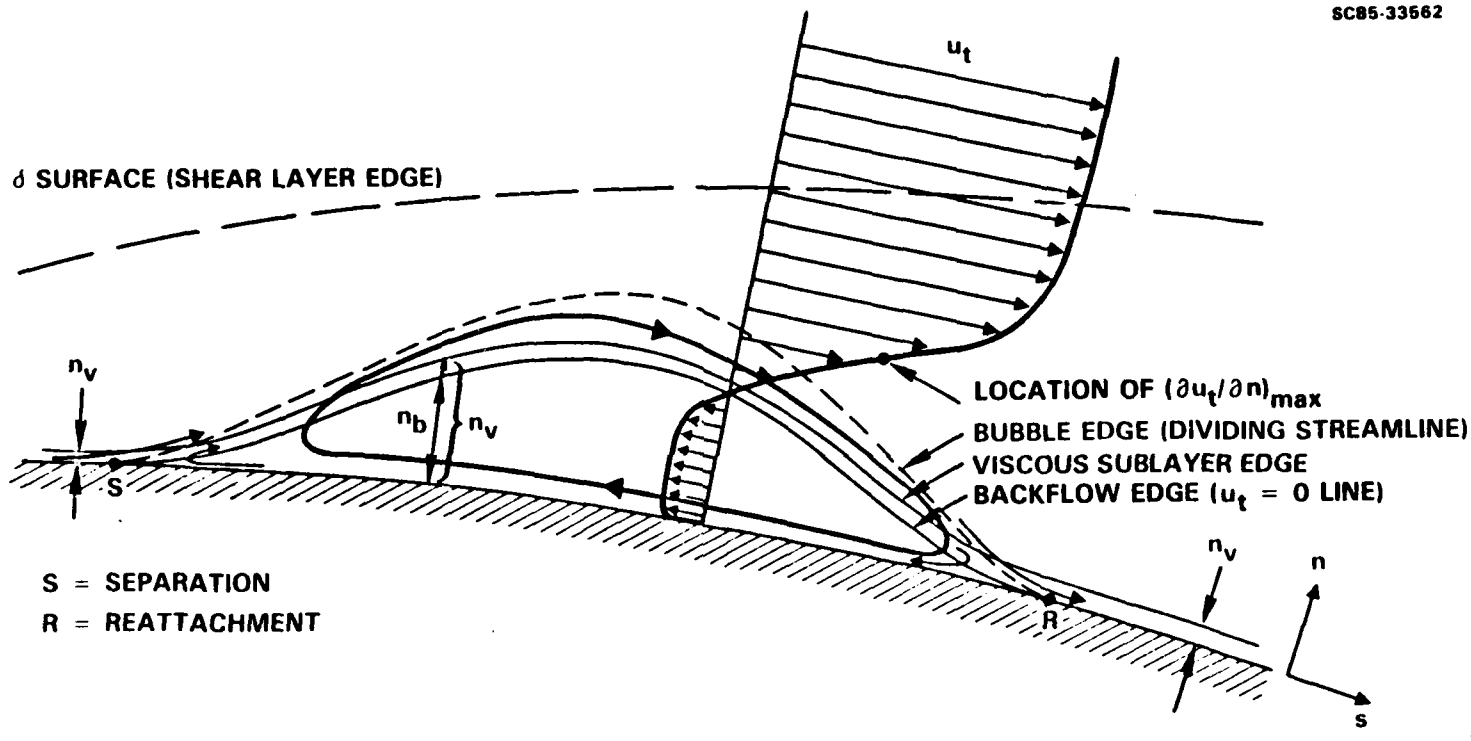

Fig. 3. Schematic view of a separated flow bubble and basic nomenclature

4. RESULTS

The computer code described previously has been applied to calculate both the internal and the external flow fields for the ramjet configuration shown in Fig. 1 under the following conditions: $M_\infty = 4.03$, $\mathrm{Re}_\infty = 7 \times 10^7$/meter. All walls were assumed to be adiabatic.

The code was applied in three modes: 1. inviscid (Euler); 2. turbulent, using the Baldwin–Lomax (B–L) model everywhere; 3. turbulent, using the B–L model outside backflow regions and the new backflow model within these regions.

Figure 4 compares internal wall pressure predictions under these three modes with experimental data from BRL[10] for a 1.7 in. injector diameter. Both the inviscid prediction and the one using the B–L model by itself are poor, grossly underpredicting the pressure rise along the cavity wall. The prediction which incorporates the backflow model, however, is much improved throughout the length of the internal wall.

Figure 5 shows skin friction distribution along the internal wall as resulting from the Mode 3 run. The extent of the reversed flow regions is clearly seen. Since the Mode 3 option proved superior to the others, all subsequent calculations were performed using this mode.

Figure 6 is a pressure contour plot for the ramjet projectile with 1.534 in. nozzle diameter and 1.9 in. injector diameter. The details of the flow field are captured very sharply, a fact which is fully attributable to the TVD scheme. Note the oblique shock in the inlet section. In Fig. 7, the inner wall pressure profile prediction is compared with the experimental data[10]. Overall, the agreement is very good, although the pressure upstream of the injector is somewhat overpredicted. This may be the result of an incorrectly predicted shape of the leading edge of the separation bubble (see next figure) which would produce an oblique shock of larger strength than the observed one. Figure 8 shows the corresponding skin friction distribution, indicating that most of the flow upstream of the injector as well as the entire cavity flow are detached from the wall.

The next calculation was done for a geometry consisting of a 1.1 in. nozzle diameter with a 1.7 in. injector diameter. The pressure contour plot of Fig. 9 clearly indicates a normal shock just upstream of the cowl inlet, a result of internal flow restriction due to the reduced nozzle throat size. This renders the flow subsonic all the way to downstream of the nozzle throat. Figure 10 shows inner wall pressure distribution for this case. Two data sets are indicated: one corresponding to the 1.1 in. nozzle diameter used in the

calculations, the other to a 1.2 in. nozzle diameter case. The predicted pressure agrees with the latter rather than with the former. Assuming that the data are reliable, this would indicate a nozzle wall displacement thickness distribution which is predicted to be thinner than the actual one. This could be the result of inadequate grid resolution on the nozzle wall, deficiency of the turbulence model, or both. Further studies will be performed to clarify this point.

Figure 11 shows the sharpness at which the normal shock is captured, a direct consequence of the TVD scheme. The figure also shows the outer wall pressure distribution in the vicinity of the cowl, where the initial rise due to the oblique shock and the subsequent drop due to the wall curvature are clearly seen. In Fig. 12, the inner wall skin friction distribution is shown. This time only the cavity flow is detached from the wall.

Finally, it was found important to indicate the sensitivity of the measured data to small changes in nozzle throat diameter. Figure 13 shows two sets of data for the 1.7 in. injector diameter case: one with a 1.534 in. nozzle throat diameter, the other with a 1.564 in. diameter. This 1.9% change produces two completely different internal flow fields, as seen by the pressure distributions. Also included in the figure is a calculation corresponding to the 1.534 in. nozzle. The pressure distribution lies between the two data sets but closer to the data corresponding to the 1.564 in. nozzle case. This sensitive range of nozzle diameters will be studied further and reported in future work.

5. CONCLUSIONS

A state–of–the–art computer code has been applied to calculate internal and external flows for a ramjet projectile under turbulent, supersonic conditions, using a multizone technique. Two types of turbulence modeling approaches were used: 1. the Baldwin–Lomax model by itself; 2. the Baldwin–Lomax model applied outside of backflow regions in conjunction with a dedicated backflow model applied within such regions. Comparison with experimental data showed a significant improvement in predictional capability when the backflow model was invoked. Since the latter model is a simple algebraic one, it should be found attractive for applications which involve recirculating flow regions. Further work is planned to assess the influence of grid resolution and turbulence modeling on the predictional capability of the code. The sensitivity of the internal flow to small changes in nozzle diameter will also be studied.

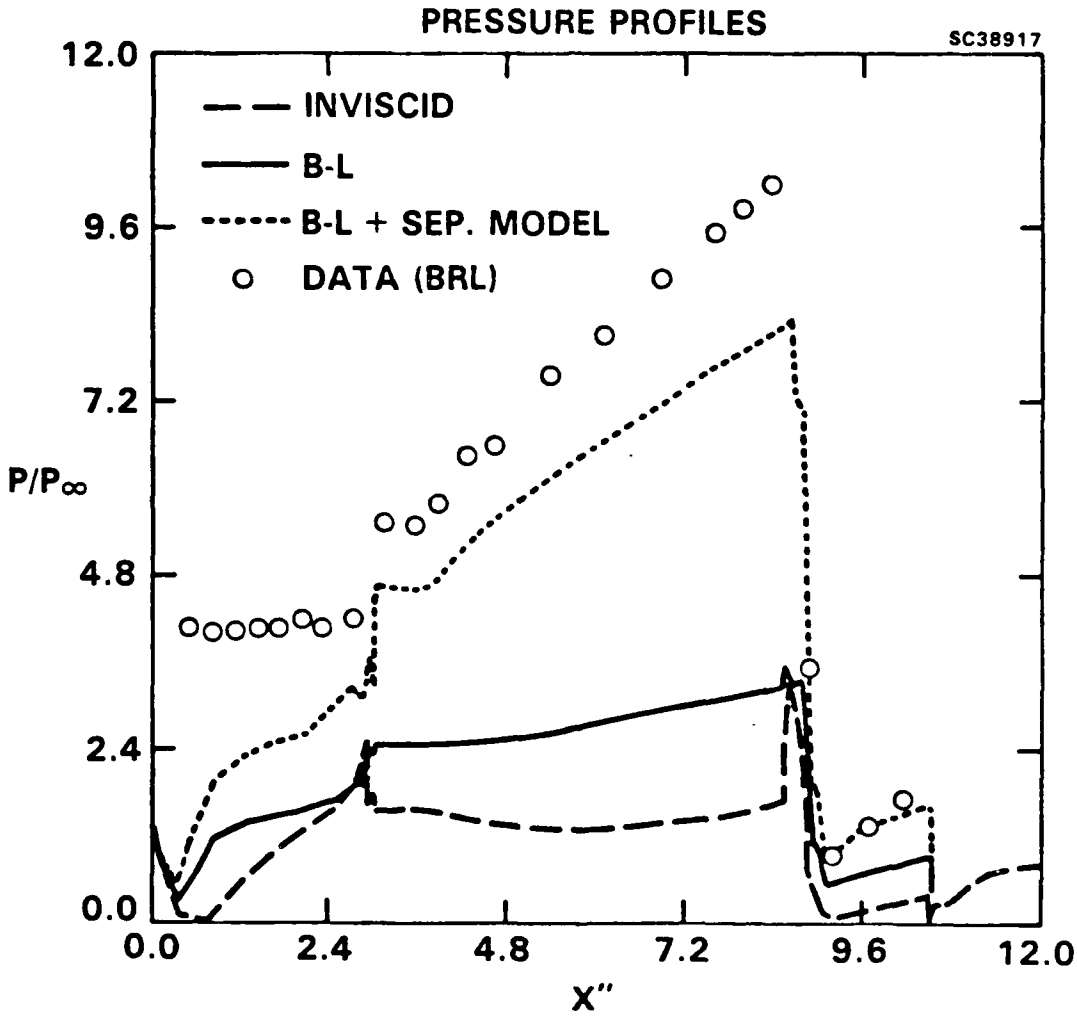

Fig. 4. Internal wall pressure distribution: calculations and data comparison

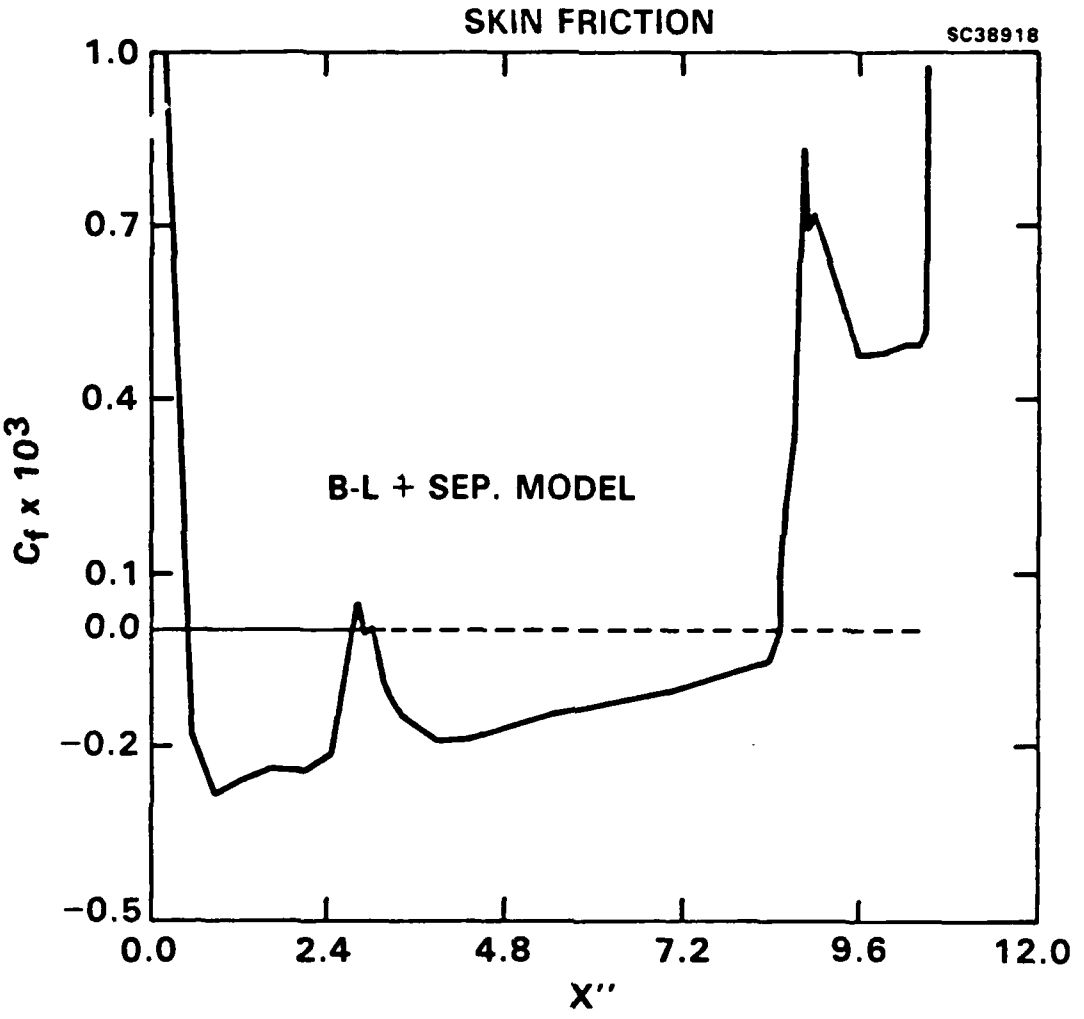

Fig. 5. Internal wall skin friction distribution

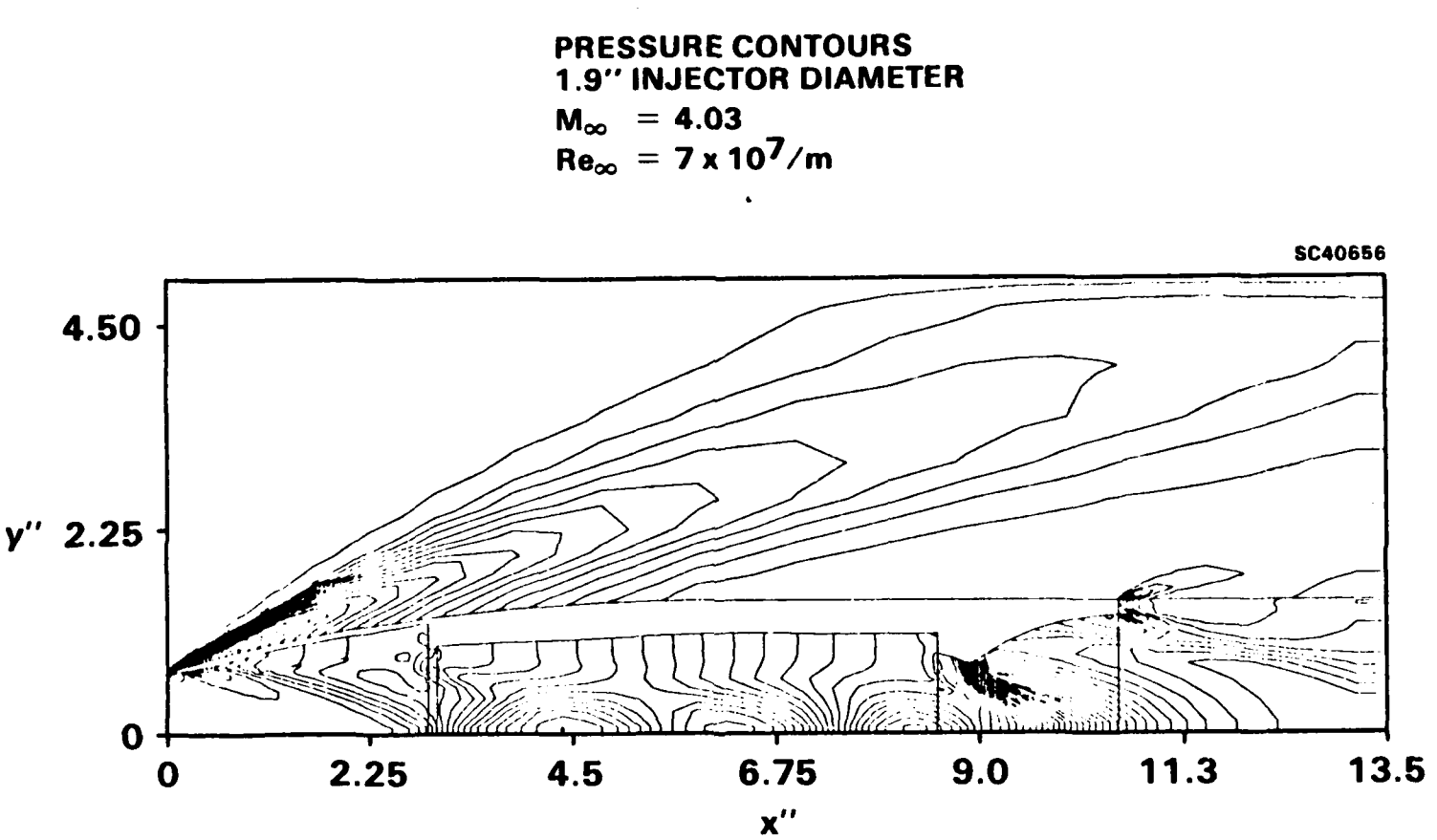

Fig. 6. Pressure contours for 1.9 in. injector geometry

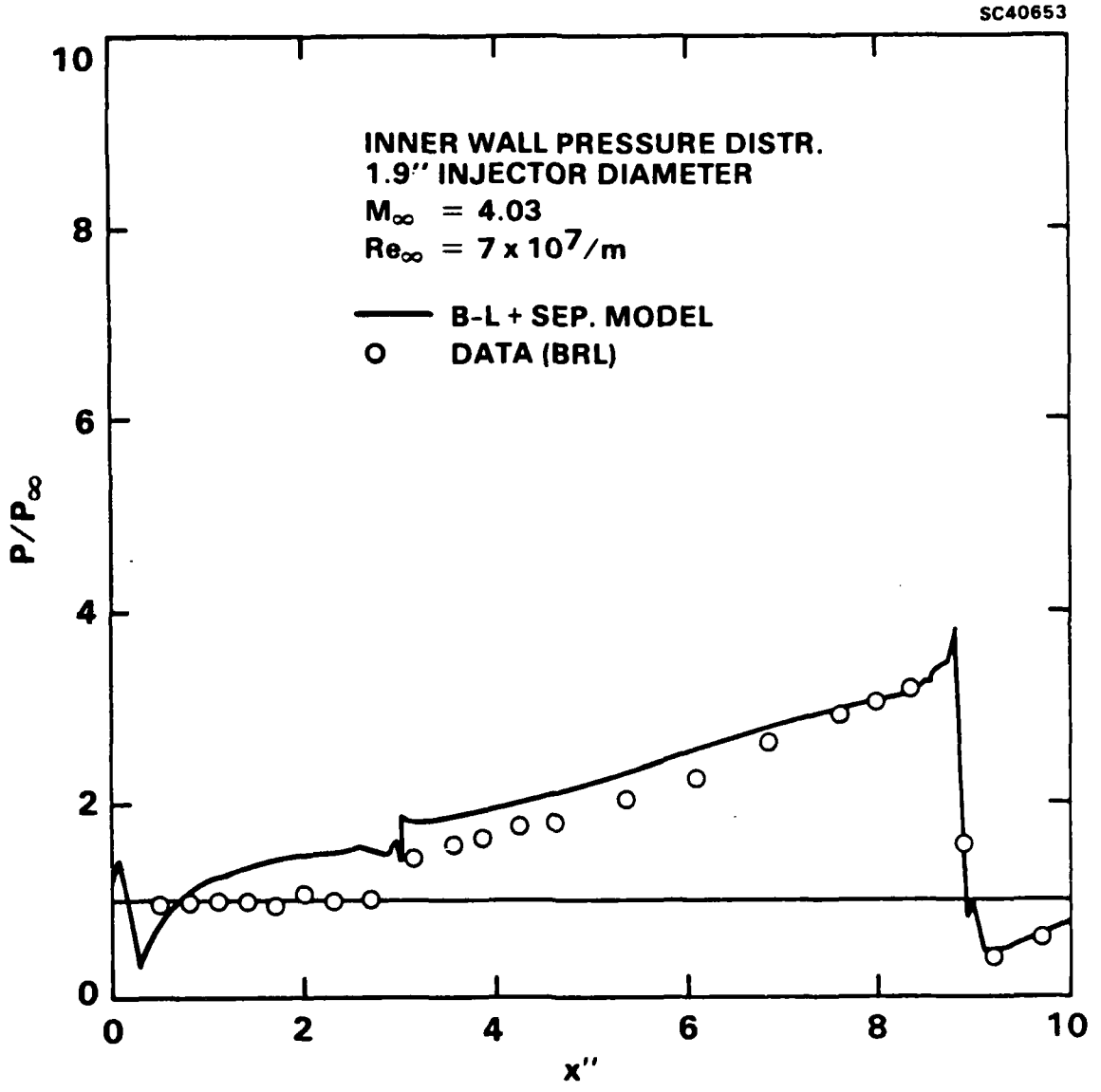

Fig. 7. Inner wall pressure distribution for 1.9 in. injector geometry

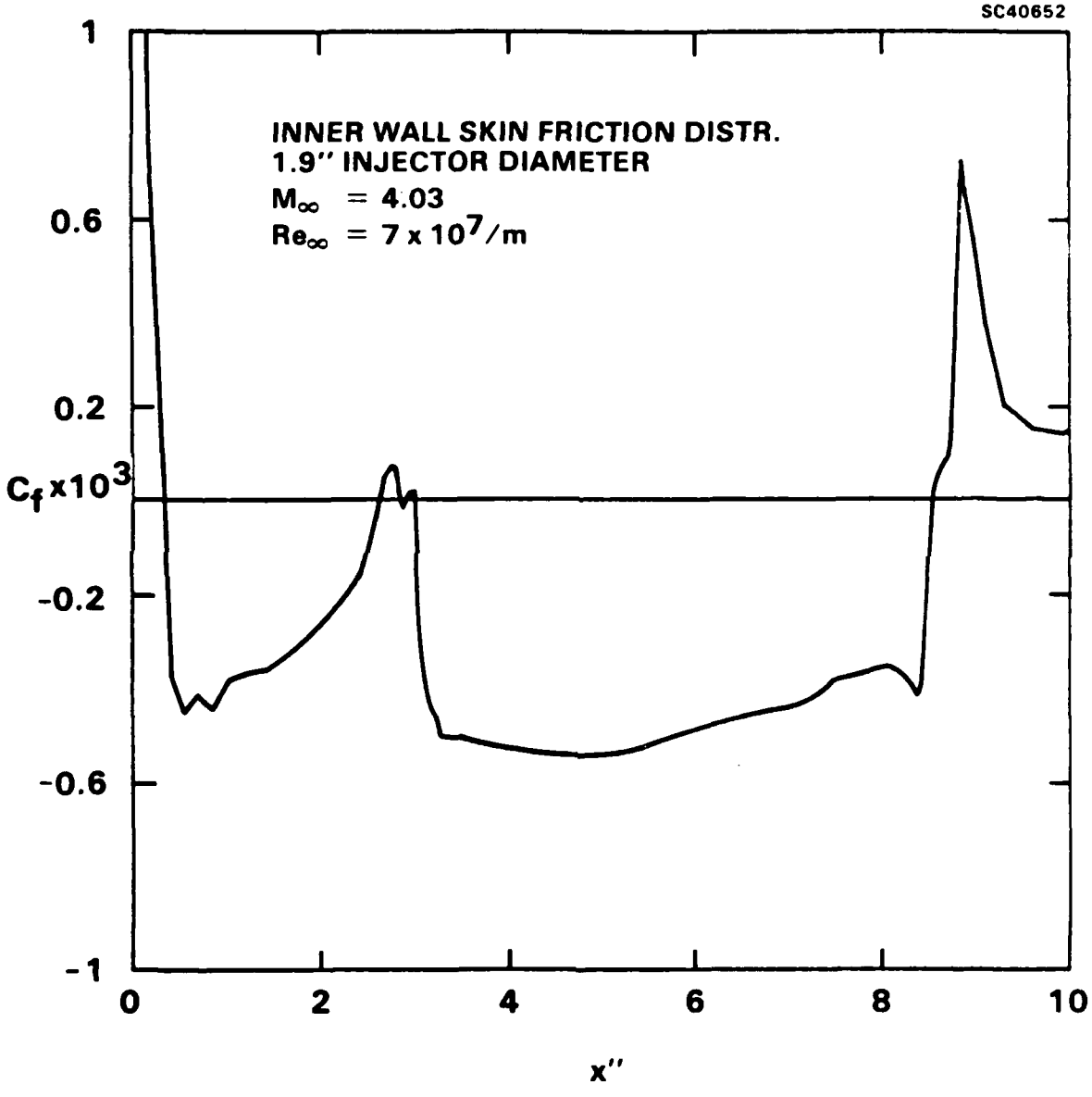

Fig. 8. Inner wall skin friction distribution for 1.9 in. injector geometry

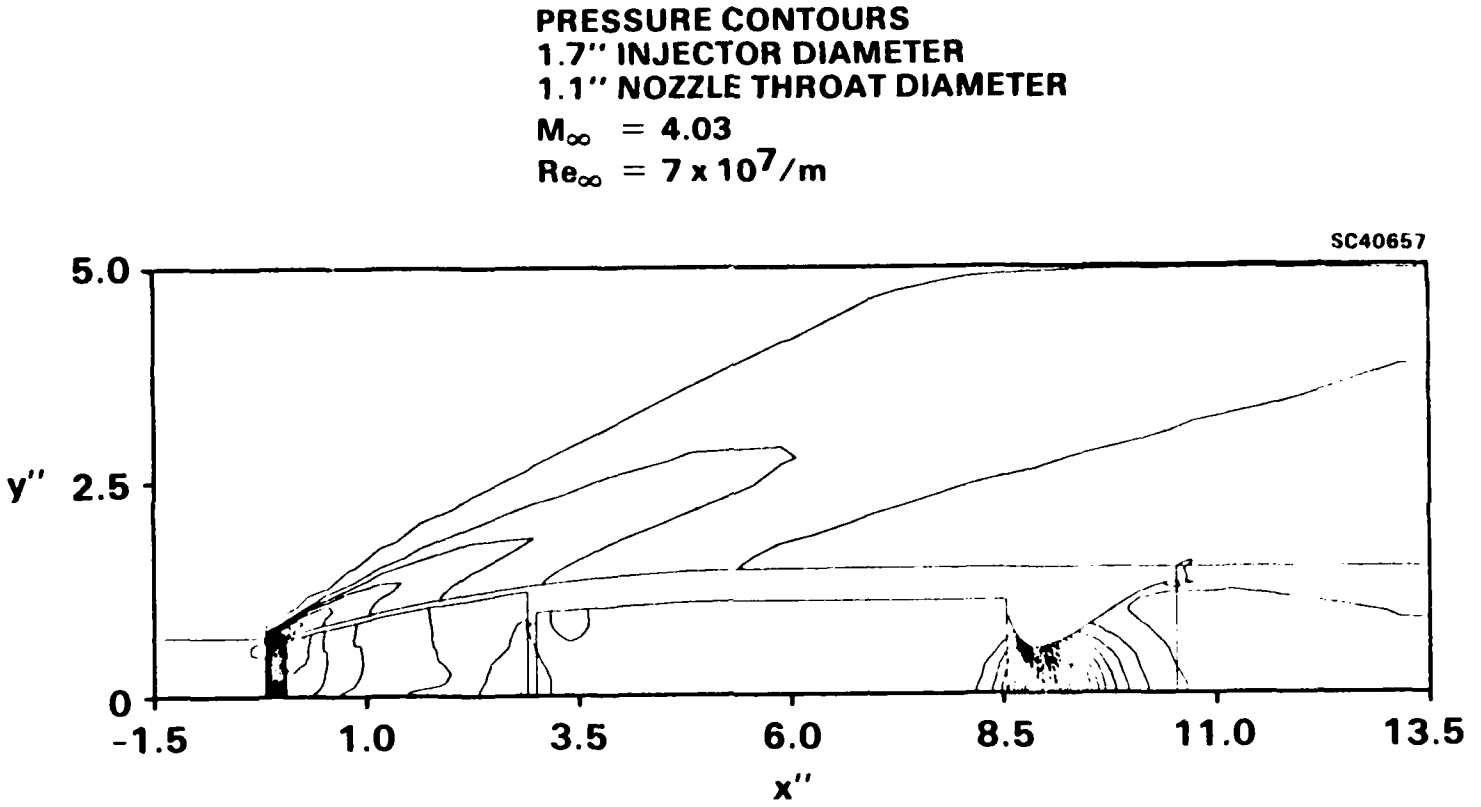

Fig. 9. Pressure contours for 1.7 in. injector/1.1 in. nozzle geometry

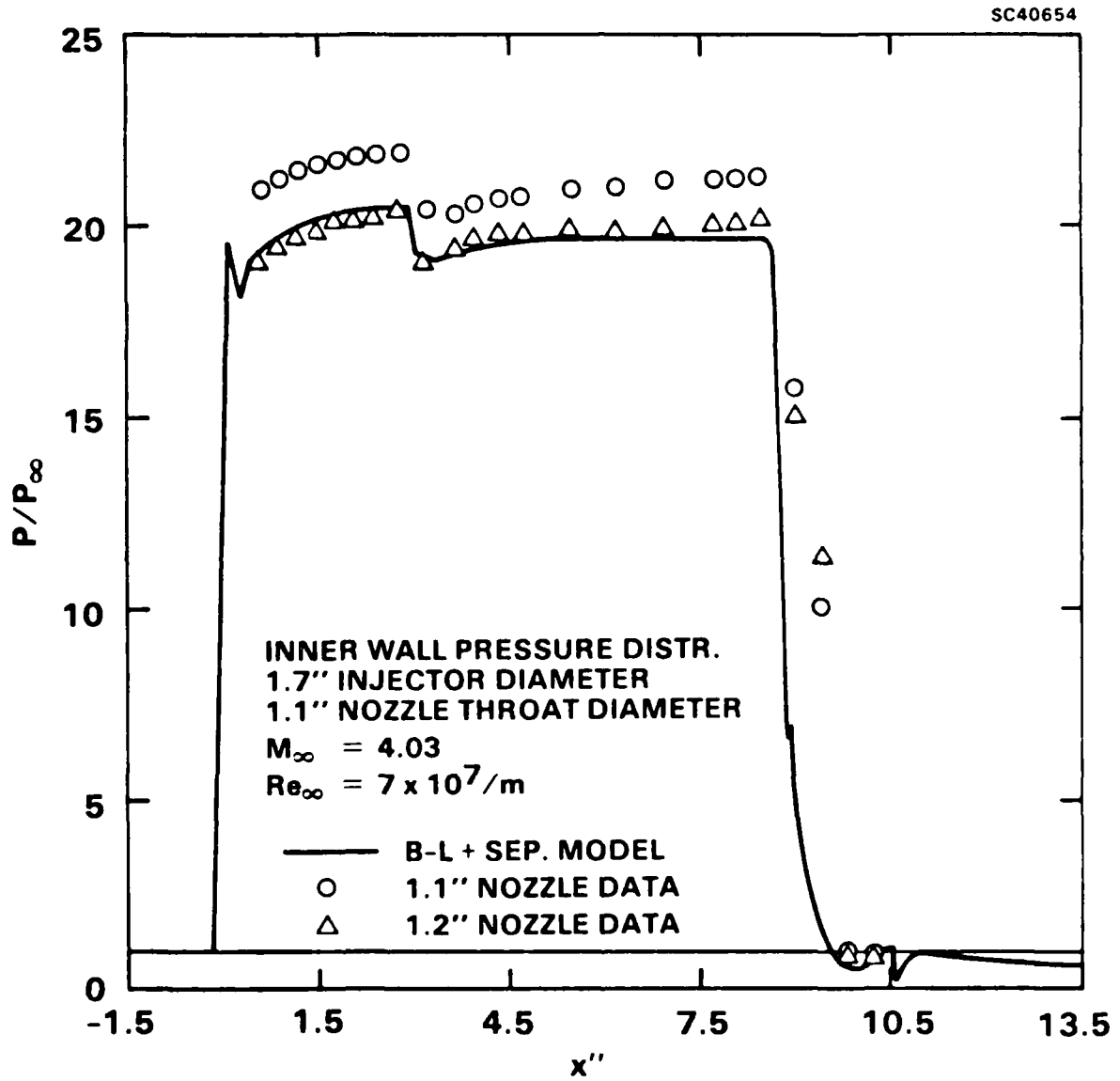

Fig. 10. Inner wall pressure distribution for 1.7 in. injector/1.1 in. nozzle geometry

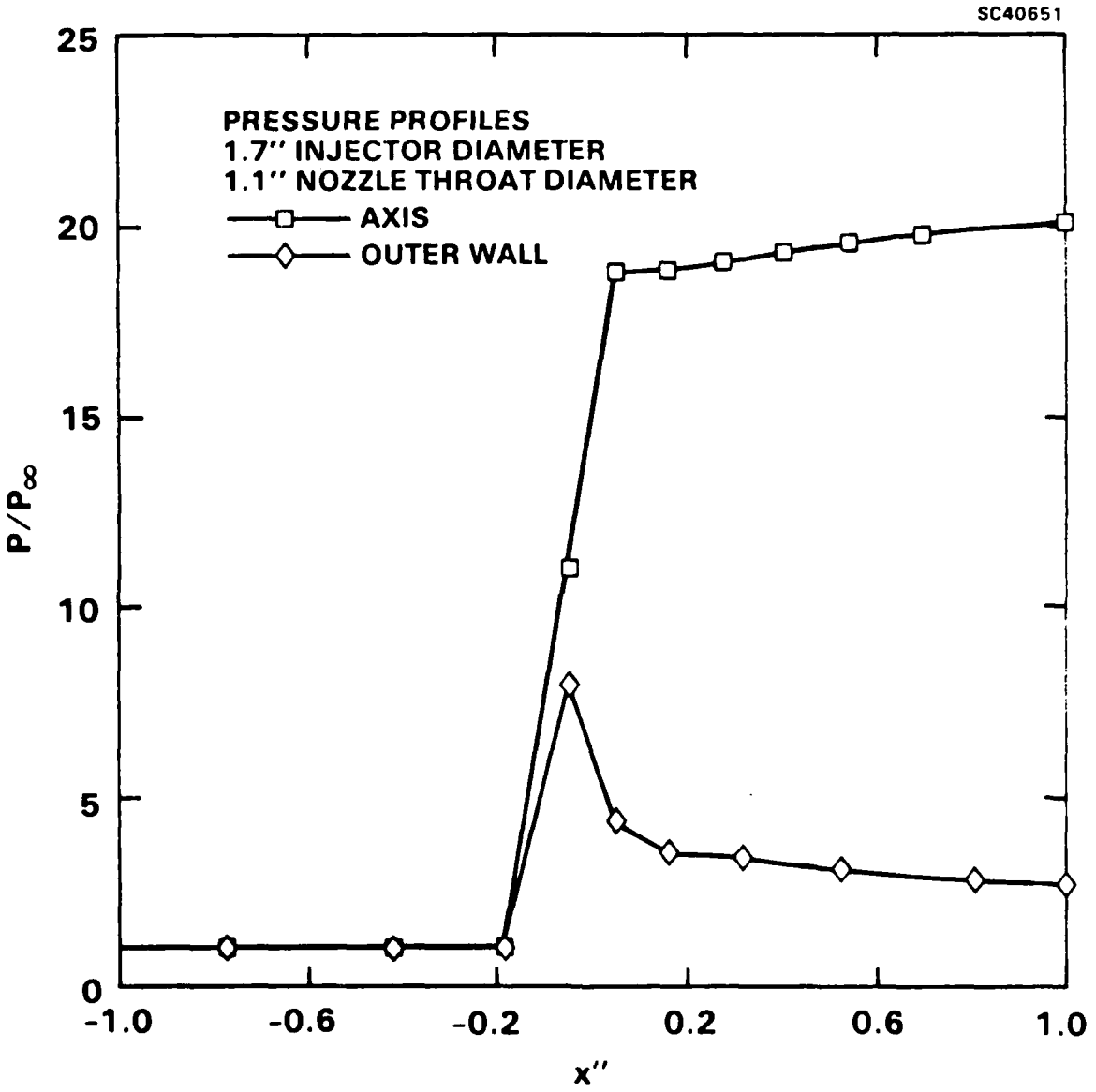

Fig. 11. Shock capturing demonstration for 1.7 in. injector/1.1 in. nozzle geometry

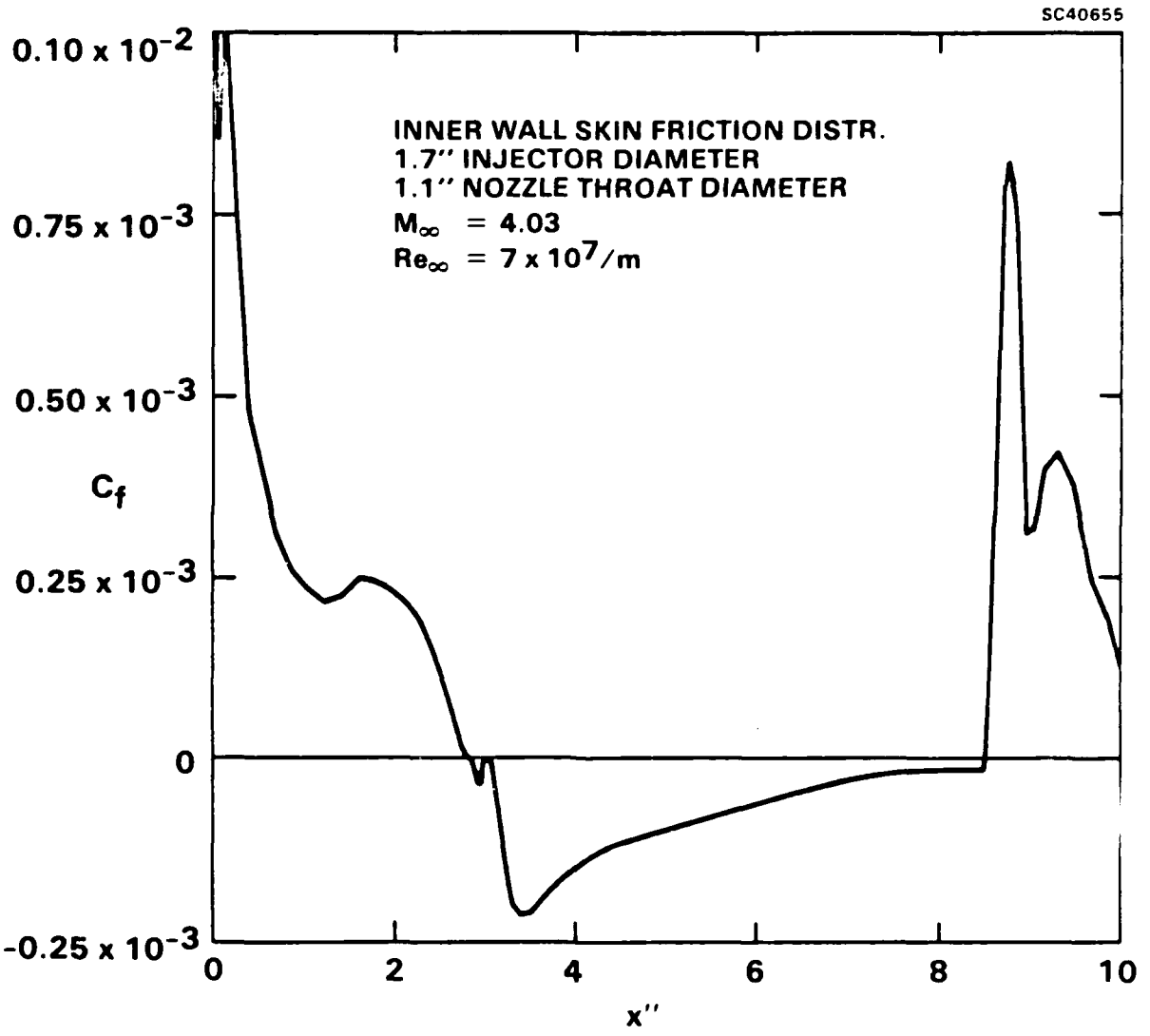

Fig. 12. Inner wall skin friction distribution for 1.7 in. injector/1.1 in. nozzle geometry

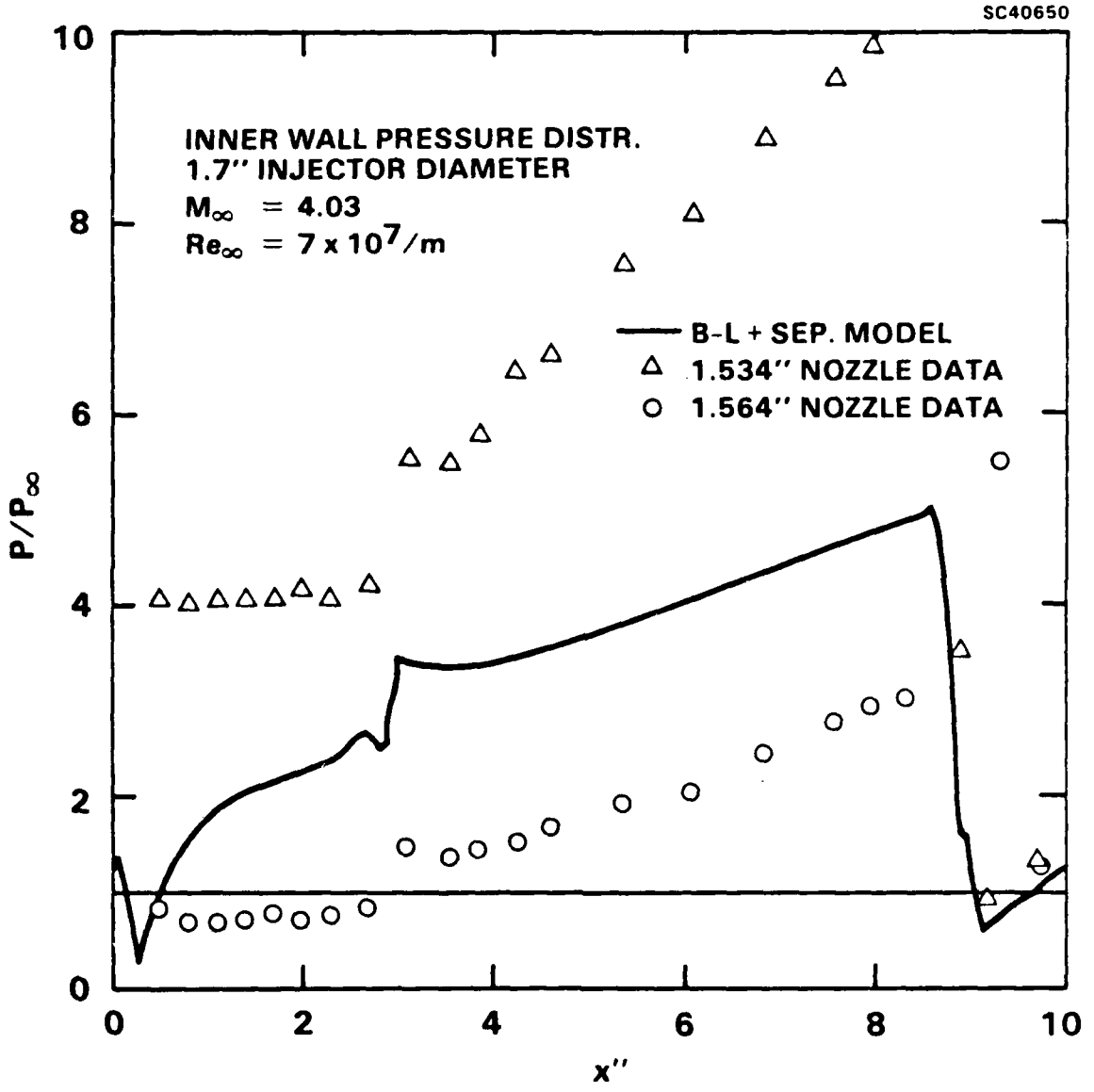

Fig. 13. Demonstration of flow sensitivity to small changes in nozzle throat size

6. REFERENCES

1. S.R. Chakravarthy and S. Osher, "A New Class of High Accuracy TVD Schemes for Hyperbolic Conservation Laws," AIAA Paper No. 85–0363, January 1985.

2. S.R. Chakravarthy, K.–Y. Szema, U.C. Goldberg, J.J. Gorski, and S. Osher, "Application of a New Class of High Accuracy TVD Schemes to the Navier–Stokes Equations," AIAA Paper No. 85–0165, January 1985.

3. S.R. Chakravarthy and K.–Y. Szema, "An Euler Solver for Three–Dimensional Supersonic Flows with Subsonic Pockets," AIAA Paper No. 85–1703, July 1985.

4. S.R. Chakravarthy, "The Versatility and Reliability of Euler Solvers Based on High–Accuracy TVD Formulations," AIAA Paper No. 86–0243, January 1986.

5. S.R. Chakravarthy, "Relaxation Methods for Unfactored Implicit Upwind Schemes," AIAA Paper No. 84–0165, January 1984. Also to appear in the *AIAA Journal*.

6. G. Mazor, G. Ben–Dor, and O. Igra, "A Simple and Accurate Expression for the Viscosity of Nonpolar Diatomic Gases up to 10,000 K," *AIAA Journal*, Vol. 23, No. 4, April 1985, pp. 636–638.

7. U.C. Goldberg, "Separated Flow Treatment with a New Turbulence Model," *AIAA Journal*, Vol. 24, No. 10, October 1986, pp. 1711–1713.

8. U.C. Goldberg, "Separated Flow Calculations with a New Turbulence Model," presented at the IACM First World Congress on Computational Mechanics, Austin, Texas, September 1986.

9. U.C. Goldberg and S.R. Chakravarthy, "Prediction of Separated Flows with a New T ılence Model," to be presented at the 5th International Conference on Numeric Methods in Laminar and Turbulent Flow, Montreal, Canada, July 1987. Also submitted to the *AIAA Journal*.

10. L.D. Kayser, R. Yalamanchili, and C. Trexler, "Pressure Measurements on the Interior Surface of a 75 mm Tubular Projectile at Mach 4," BRL–IMR–855, U.S. Army Ballistic Research Laboratory, Aberdeen Proving Ground, Maryland, October 1985.

APPENDIX

A SUMMARY OF BACKFLOW TURBULENCE MODEL EQUATIONS

Following are the most important equations on which the separation turbulence model is based.

k and ϵ within the separation bubble are given by

$$\rho k/\rho_b k_b = \left[e^{\phi}/(e^{\phi}-1)\right]\left[1-e^{-\phi(n/n_b)^2}\right]$$
$$\equiv \mathcal{G}(s,n) \quad , \quad 0 \le n \le n_b,$$

$$(\rho/\rho_b)^{3/2}\epsilon = \left[k_v \mathcal{G}(s,n)\right]^{3/2}/n_v \quad , \quad 0 \le n \le n_b,$$

where

$$\phi = 0.5\,,\ \beta \equiv k_v/k_b = 1+\left[(n_v/n_b)^2-1\right]\phi/(e^{\phi}-1)\,,$$
$$\rho_v k_v/\rho_w = u_s^2/\sqrt{C_\mu^* n_v^*} = 20C_\mu^{1/4}+n_b^* \quad ,$$
$$n^* \equiv n u_s/\nu_w \quad , \quad C_\mu = 0.09 \quad , \quad C_\mu^* = 0.7\,,$$

and $u_s = \left(\overline{-u'v'}\right)_{\max}^{1/2} = \left[\nu_{t,m}(\partial u_t/\partial n)_{\max}\right]^{1/2}$. Here, $\left(\overline{-u'v'}\right)_{\max}$ is the maximum Reynolds stress, assumed to correspond to the maximum normal-to-wall mean velocity gradient. $\nu_{t,m}$ is the value of eddy viscosity where the aforementioned maximum gradient occurs (see Fig. 3), and it must be supplied by the turbulence model which is applied external to the separation bubble.

The length scale of turbulence within the bubble is given by $L = n_v/\beta^{3/2}$.

Finally, eddy viscosity is given by

$$\nu_t/\nu_w = \sqrt{\frac{\rho_w}{\rho}}\left[f(n/n_b)/(2\sqrt{2}\beta^2)\right] n_v^* \mathcal{G}^{1/2}(s,n) \quad ,$$
$$0 \le n \le n_b$$

where $f(n/n_b) = A(n/n_b)+B, A = -(C_\mu^*/2)^{9/5}\,,\ B = (C_\mu^*/2)^{3/5} - A.$

DISTRIBUTION LIST

No. Copies	Organization
12	Administrator Defense Technical Information Center ATTN: DTIC-FDAC Cameron Station, Bldg. 5 Alexandria, VA 22304-6145
1	HQDA DAMA-ART-M Washington, DC 20310
1	Commander US Army Materiel Command ATTN: AMCDRA-ST 5001 Eisenhower Avenue Alexandria, VA 22333-0001
1	Commander US Army ARDEC ATTN: SMCAR-TDC Picatinny Arsenal, NJ 07806-5000
1	Commander U.S. Armament RD&E Center US Army AMCCOM ATTN: SMCAR-MSI Picatinny Arsenal, NJ 07806-5000
1	Commander U.S. Armament RD&E Center US Army AMCCOM ATTN: SMCAR-LC Picatinny Arsenal, NJ 07806-5000
1	Commander U.S. Army AMCCOM ATTN: SMCAR-CAWS-AM Mr. DellaTerga Picatinny Arsenal, NJ 07806-5000
1	OPM Nuclear ATTN: AMCPM-NUC COL. W. P. Farmer Dover, NJ 07801-5001
1	AFWL/SUL Kirtland AFB, NM 87117-6008
3	Commander U.S. Armament RD&E Center US Army AMCCOM ATTN: SMCAR-AET-A Mr. R. Kline ATTN: SMCAR-AET Mr. F. Scerbo Mr. J. Bera Picatinny Arsenal, NJ 07806-5000
1	Commander US Army Armament, Munitions and Chemical Command ATTN: AMSMC-IMP-L Rock Island, IL 61299-7300
1	Commander U.S. AMCCOM ARDEC CCAC Benet Weapons Laboratory ATTN: SMCAR-CCB-TL Watervliet, NY 12189-4050
1	Commander US Army Aviation Systems Command ATTN: AMSAV-ES 4300 Goodfellow Blvd St Louis, MO 63120-1789

DISTRIBUTION LIST

No. Copies	Organization
1	Director US Army Aviation Research and Technology Activity Moffett Field, CA 94035-1099
1	Commander US Army Communications Electronics Command ATTN: AMSEL-ED Fort Monmouth, NJ 07703-5000
1	Commander CECOM R&D Technical Library ATTN: AMSEL-IM-L, (Reports Section) B. 2700 Fort Monmouth, NJ 07703-5000
10	C. I. A. OIC/DB/Standard GE47 HQ Washington, DC 20505
1	Commandant US Army Infantry School ATTN: ATSH-CD-CS-OR Fort Benning, GA 31905-5400
1	Commander US Army Missile Command Research Development and Engineering Center ATTN: AMSMI-RD Redstone Arsenal, AL 35898-5230
1	Commander US Army Missile Command ATTN: AMSMI-RDK, Mr. Dahlke Redstone Arsenal, AL 35898-5230
1	Director US Army Missile and Space Intelligence ATTN: AIAMS-YDL Redstone Arsenal, AL 35898-5500
1	Commander US Army Tank Automotive Command ATTN: AMSTA-TSL Warren, MI 48397-5000
1	Director US Army TRADOC Analysis Center ATTN: ATOR-TSL White Sands Missile Range NM 88002-5502
1	Commander US Army Development & Employment Agency ATTN: MODE-ORO Fort Lewis, WA 98433-5000
1	Commandant US Army Field Artillery School ATTN: ATSF-GD Fort Sills, OK 73503
1	Director National Aeronautics and Space Administration Langley Research Center ATTN: Tech Library Langley Station Hampton, VA 23365
1	Director US Army Field Artillery Board ATTN: ATZR-BDW Fort Sills, OK 73503

DISTRIBUTION LIST

No. Copies	Organization
1	Commander US Army Dugway Proving Ground ATTN: STEDP-MT Mr. G. C. Travers Dugway, UT 84022
1	Commander US Army Yuma Proving Ground ATTN: STEYP-MTW Yuma, AZ 85365-9103
2	Director Sandia National Laboratories ATTN: Dr. W. Oberkampf Dr. W. P. Wolfe Division 1636 Albuquerque, NM 87185
1	Air Force Armament Laboratory ATTN: AFATL/DLODL (Tech Info Center) Eglin AFB, FL 32542-5438
1	Commander Naval Surface Weapons Center ATTN: Dr. W. Yanta Aerodynamics Branch K-24, Building 402-12 White Oak Laboratory Silver Spring, MD 20910
1	Aerospace Corporation Aero-Engineering Subdivision ATTN: Walter F. Reddall El Segundo, CA 90245
1	Director National Aeronautics and Space Administration Marshall Space Flight Center ATTN: Dr. W. W. Fowlis Huntsville, AL 35812
1	Director National Aeronautics and Space Administration Ames Research Center ATTN: Dr. J. Steger Moffet Field, CA 94035
1	Calspan Corporation ATTN: W. Rae P.O. Box 400 Buffalo, NY 14225
3	Rockwell International ATTN: Dr. V. Shankar Dr. S. Chakravarthy Dr. U. Goldberg 1049 Camino Dos Rios Thousand Oaks, CA 91360
1	University of Santa Clara Department of Physics ATTN: R. Greeley Santa Clara, CA 95053
1	Arizona State University Department of Mechanical and Energy Systems Engineering ATTN: G.P. Neitzel Tempe, AZ 85281

DISTRIBUTION LIST

No. Copies	Organization
1	Massachusetts Institute of Technology ATTN: H. Greenspan 77 Massachusetts Avenue Cambridge, MA 02139
1	North Carolina State University Mechanical and Aerospace Engineering Department ATTN: F.F. DeJarnette Raleigh, NC 27607
1	Northwestern University Department of Engineering Science and Applied Mathematics ATTN: Dr. S.H. Davis Evanston, IL 60201
1	University of Colorado Department of Astro-Geophysics ATTN: E.R. Benton Boulder, CO 80302
2	University of Maryland ATTN: W. Melnik J.D. Anderson College Park, MD 20740
1	University of Maryland Baltimore County Department of Mathematics ATTN: Dr. Y.M. Lynn 5401 Wilkens Avenue Baltimore, MD 21228
1	Rensselaer Polytechnic Institute Department of Math Sciences Troy, NY 12181

No. Copies	Organization
1	Director Lawrence Livermore National Laboratory ATTN: Mail Code L-35 Mr. T. Morgan P.O. Box 808 Livermore, CA 94550
1	University of California - Davis ATTN: Dr. Harry A. Dwyer Davis, CA 95616
1	Director Johns Hopkins University Applied Physics Laboratory ATTN: Dr. Fred Billig John Hopkins Rd. Laurel, MD 20707
1	Commander Defense Advanced Research Projects Agency ATTN: MAJ. R. Lundberg 1400 Wilson Blvd. Arlington, VA 22209
1	Hughes Aircraft ATTN: Dr. John McIntyre Mail Code S41/B323 P.O. Box 92919 Los Angeles, CA 90009

DISTRIBUTION LIST

No. Copies	Organization
1	Interferometrics Inc. ATTN: Mr. R. F. L'Arriva 8150 Leesburg Pike Vienna, VA 22180
1	United Technologies Chemical Systems Division ATTN: Mr. A. L. Holzman 1050 East Arques P.O. Box 358 Sunnyvale, CA 94086

No. Copies	Organization
	Aberdeen Proving Ground
	Director, USAMSAA ATTN: AMXSY-D AMXSY-RA, R. Scungio
	Commander, UASTECOM ATTN: AMSTE-SI-F AMSTE-TE-F, W. Vomocil PM-SMOKE, Bldg. 324 ATTN: AMCPM-SMK-M Mr. J. Callahan
	Cdr, CRDC, AMCCOM ATTN: SMCCR-MU Mr. W. Dee Mr. C. Hughes Mr. D. Bromley ATTN: SMCCR-RSP-A Mr. Miles Miller Mr. Donald Olson ATTN: SMCCR-SPS-IL SMCCR-RSP-A SMCCR-MU

USER EVALUATION SHEET/CHANGE OF ADDRESS

This Laboratory undertakes a continuing effort to improve the quality of the reports it publishes. Your comments/answers to the items/questions below will aid us in our efforts.

1. BRL Report Number_____ Date of Report_____

2. Date Report Received_____

3. Does this report satisfy a need? (Comment on purpose, related project, or other area of interest for which the report will be used.)_____

4. How specifically, is the report being used? (Information source, design data, procedure, source of ideas, etc.)_____

5. Has the information in this report led to any quantitative savings as far as man-hours or dollars saved, operating costs avoided or efficiencies achieved, etc? If so, please elaborate._____

6. General Comments. What do you think should be changed to improve future reports? (Indicate changes to organization, technical content, format, etc.)

CURRENT ADDRESS

Name

Organization

Address

City, State, Zip

7. If indicating a Change of Address or Address Correction, please provide the New or Correct Address in Block 6 above and the Old or Incorrect address below.

OLD ADDRESS

Name

Organization

Address

City, State, Zip

(Remove this sheet, fold as indicated, staple or tape closed, and mail.)